ACS APPLIED ENERGY MATERIALS
Cite This: ACS Appl. Energy Mater. 2019, 2, 1452−1459
Article
www.acsaem.org

Interface-Enabled Ion Conduction in $Li_{10}GeP_2S_{12}$−Poly(ethylene Oxide) Hybrid Electrolytes

Jin Zheng,[†] Pengbo Wang,[†] Haoyu Liu,[†] and Yan-Yan Hu*[,†,‡]

[†]Department of Chemistry and Biochemistry, Florida State University, Tallahassee, Florida 32306, United States
[‡]Center of Interdisciplinary Magnetic Resonance, National High Magnetic Field Laboratory, Tallahassee, Florida 32310, United States

Supporting Information

ABSTRACT: Organic−inorganic hybrid solid electrolytes are expected to integrate the merits of both moieties for addressing the challenges in achieving fast ion conduction and high stability for energy storage applications. $Li_{10}GeP_2S_{12}$ (LGPS)-poly(ethylene oxide) (PEO) (bis(trifluoromethane)sulfonimide lithium (LiTFSI)) hybrid electrolytes have been prepared, which exhibit ionic conductivities up to 0.22 mS cm^{-1} and good long-term cycling stability against Li-metal. High-resolution solid-state ^{6}Li NMR is employed to examine the local structural environments of Li ions in the LGPS-PEO (LiTFSI) hybrids, which identifies Li ions from PEO (LiTFSI), in bulk LGPS, and at LGPS-PEO interfaces. Tracer-exchange Li NMR reveals that Li ions transport mainly through LGPS-PEO interfaces. The impact of LGPS and LiTFSI contents on the interface chemistry within LGPS-PEO hybrid electrolytes has been examined. The measured conductivities of LGPS-PEO hybrids positively correlate with the available Li ions at LGPS-PEO interfaces. This study provides insights for engineering interfaces in organic−inorganic hybrids to develop high-performance electrolytes for solid-state rechargeable batteries.

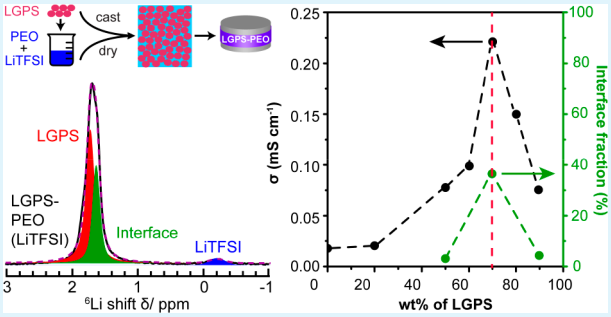

KEYWORDS: *interface chemistry, hybrid electrolytes, fast ion conduction, tracer-exchange NMR*

INTRODUCTION

Rechargeable Li-ion batteries (LIBs) are widely utilized in many portable electronics and electric vehicles. In conventional rechargeable LIBs, electrolytes are made of Li salts dissolved in organic solvents. The thermal and electrochemical instabilities of these organic solvents lead to severe safety issues. As promising alternatives, solid electrolytes are nonflammable, stable, and energy dense.[1]

Solid electrolytes are classified into three categories, namely, polymers, inorganics, and composite electrolytes. Polymer electrolytes have shown good flexibility and processability, but they suffer from low ionic conductivity at room temperature. Inorganic electrolytes often exhibit high ionic conductivity; however, their applications are impeded by poor mechanical properties and poor wettability. Composite electrolytes integrating the merits of inorganic and polymer electrolytes have attracted a lot of attention in both fundamental studies and practical applications.[2,3]

Poly(ethylene oxide) (PEO) is often used for fabricating composite electrolytes because of its favorable characteristics such as low cost, flexibility, processability, and high Li-ion solvating capability.[4] Most PEO-based composites employ inorganic fillers for enhancing the ionic conductivity of PEO. These inorganic fillers decrease the crystallinity of polymers, which results in desirable segmental motions for ion conduction.[4] Moreover, inorganic fillers can facilitate the dissociation of ion pairs to release free Li^+ and trap anions in Li salts to increase transference number.[5,6] Compared with polymer electrolytes, polymer−filler composite electrolytes exhibit increased Young's modulus, which is believed to suppress the growth of Li dendrites.[7,8]

Among inorganic electrolytes, sulfides exhibit high ionic conductivities comparable to liquid electrolytes.[9] Sulfides are soft with much lower grain boundary resistance compared with oxides, such as garnets. Notably, $Li_{10}GeP_2S_{12}$ (LGPS) shows a high ionic conductivity of 12 mS cm^{-1} at room temperature and an electrochemical stability window of 0−4 V versus Li^+/Li.[10] However, LGPS is not stable against lithium metal.[11] Prior work from our group has demonstrated that PEO coating on LGPS pellets improves the stability at the electrode−electrolyte interface and helps to maintain Li distribution homogeneity.[12]

In the examples of composite electrolytes mentioned above, they all have one dominant component and ion conduction mainly occurs either in the polymer or inorganic phase; the synergies at the organic−inorganic interfaces are not achieved or investigated. In this work, we developed a hybrid electrolyte imbedding a comparable amount of LGPS into the PEO

Received: November 20, 2018
Accepted: January 18, 2019
Published: January 18, 2019

DOI: 10.1021/acsaem.8b02008
ACS Appl. Energy Mater. 2019, 2, 1452−1459

matrix, examined the roles of LGPS-PEO interfaces in ion conduction, and studied the impact of composition and lithium salt content on interface chemistry, ion conductivity, and stability. We have employed high-resolution solid-state NMR coupled with $^{6}Li \rightarrow {}^{7}Li$ tracer-exchange to understand the fundamental science that drives the enhanced ion conduction and long-term cycling stability.[13−16]

EXPERIMENTAL SECTION

Synthesis of LGPS. Considering the sensitivity of the material to oxygen and moisture, the sample preparation process was performed in an Ar-filled glovebox (O_2 and H_2O < 0.1 ppm). Li_2S (99.98%, Sigma-Aldrich), P_2S_5 (99%, Sigma-Aldrich), and GeS_2 (>99%, Santa Cruz Biotechnology) were weighed out with a mole ratio of 5:1:1. The precursor materials were transferred to a ZrO_2 jar with ZrO_2 balls and ball-milled with a SPEX SamplePrep 8000 M apparatus for 2 h. The powder appeared to be brown. The as-prepared powder was heated in a quartz tube at 550 °C for 12 h with a temperature ramp of 1 °C min^{-1} and gradually cooled to room temperature. The color of the final product was gray.

Preparation of Hybrid Electrolytes. The PEO (LiTFSI) solution of different Li-salt concentrations (EO/Li = 18:1, 12:1, 9:1, or 6:1) was prepared by dissolving lithium bis-(trifluoromethanesulfonyl)imid (LiTFSI) (Sigma-Aldrich) and PEO (Sigma-Aldrich, Mw = 400000) in anhydrous acetonitrile. The LiTFSI and PEO were dried at 90 and 50 °C, respectively, for 12 h before use. The solutions were stirred overnight to obtain homogeneous distribution of Li salts. The LGPS-PEO (LiTFSI) hybrid electrolyte films were prepared via a conventional solution-casting method. The mixture of LGSP and PEO (LiTFSI) with different LGPS fractions (20, 50, 60, 70, 80, or 90 wt %) was ball-milled at 200 rpm for 2 h. The homogeneous slurry was then cast on a flat Teflon plate with a doctor blade and then dried in an Ar-filled glovebox at room temperature (22 °C) for 24 h.

Electrochemical Measurements. The LGPS-PEO (LiTFSI) hybrid films were punched into discs and assembled into symmetric cells with stainless steel pieces as blocking electrodes for electrochemical impedance spectroscopy (EIS) measurements. The EIS measurements were performed on a Gamry Reference 600+ with a frequency range from 5 MHz to 1 Hz. The ionic conductivity (σ) was calculated with $\sigma = L/(R \times A)$, where L is the thickness of the electrolyte in centimeters, R the resistance in ohms, and A the contact area of the electrolyte and the electrodes in centimeters squared (cm^2). The conductivity of LGPS-PEO (LiTFSI) and PEO (LiTFSI) was measured over the temperature range of 20 to 80 °C for the Arrhenius plots. To test the electrochemical stability of LGPS, PEO (LiTFSI), and LGPS-PEO (LiTFSI) against Li metal, Li metal foils were used as working electrodes in the symmetric cells. Cyclability tests were carried out on an Arbin (BT2043) battery testing system with a current density of 10 μA cm^{-1}, which switched the sign every hour.

Isotope Exchange. Isotope exchange, $^{6}Li \rightarrow {}^{7}Li$, was employed to track Li-ion pathways in the LGPS-PEO (LiTFSI) hybrid electrolytes. A biased current was applied on the cell, $^{6}Li|LGPS\text{-}PEO\ (LiTFSI)|^{6}Li$, to drive ^{6}Li ions from the electrodes to pass through the electrolyte, partially replacing ^{7}Li ions on their way.

Solid-State NMR Measurements. $^{6,7}Li$ magic-angle-spinning (MAS) NMR and $^{1}H-{}^{6}Li$ cross-polarization (CP) NMR experiments were performed on a Bruker Avance III-500 spectrometer with a ^{6}Li Larmor frequency of 73.6 MHz and a ^{7}Li Larmor frequency of 194.4 MHz. LGPS-PEO (LiTFSI) hybrid samples were packed in 2.5 mm rotors and spun at a speed of 25 kHz for $^{6,7}Li$ NMR and 10 kHz for $^{1}H-{}^{6}Li$ CP NMR. For ^{6}Li NMR, the 90° pulse length was 4.75 μs, and the recycle delay was 100 s. For ^{7}Li NMR, the 90° pulse length was 2.0 μs and the recycle delay was 100 s. For $^{1}H-{}^{6}Li$ CP NMR, the ^{1}H 90° pulse length was 2.55 μs and the recycle delay was 2 s. The contact time of $^{1}H-{}^{6}Li$ CP NMR varied from 0.2 to 7 ms. Chemical shifts were referenced to solid LiCl at 0 ppm. The fitting parameters are listed in Table S1.

RESULTS AND DISCUSSION

The preparation process of LGPS-PEO (LiTFSI) hybrid electrolytes is illustrated in Figure 1 and described in the Experimental Section. The resulting hybrid films are flexible with a thickness of around 100 μm. The scanning electron microscopy (SEM) image of 70 wt % LGPS-PEO (LiTFSI) (9:1) is shown in Figure S1, which reveals that LGPS particles are homogeneously dispersed within PEO matrix and the particle size of LGPS is around 25 nm. The hybrid films are sandwiched between two blocking electrodes made of stainless-steel disks for conductivity measurements using electrochemical impedance spectroscopy (EIS) or between two Li metal foils for electrochemical stability tests.

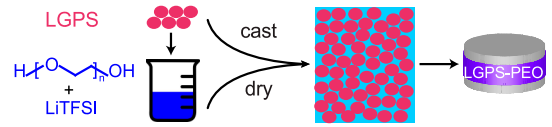

Figure 1. Schematic illustrating the preparation process of LGPS-PEO (LiTFSI) hybrid films and the symmetric battery cells that use LGPS-PEO (LiTFSI) as electrolytes.

To probe the structural environments of Li ions in LGPS-PEO (LiTFSI) hybrid electrolytes, high-resolution solid-state magic-angle-spinning (MAS) ^{6}Li NMR is employed. LiTFSI, PEO (LiTFSI), and pure LGPS are used as reference samples to facilitate identifications of structural environments in LGPS-PEO (LiTFSI) based on NMR studies (Figure 2). The ^{6}Li chemical shifts of Li in LiTFSI and pristine LGPS are −0.16 and 1.70 ppm, respectively. The signal of Li in PEO (LiTFSI) moves downfield to 0.30 ppm due to the interactions between Li^+ and PEO. After PEO (LiTFSI) is mixed with LGPS powders, the NMR resonance from Li^+ in LiTFSI shifts back to −0.16 ppm, an indication of weakened interactions between Li^+ and PEO. The broadening of this resonance suggests a more disordered local structural environment of Li^+, likely at

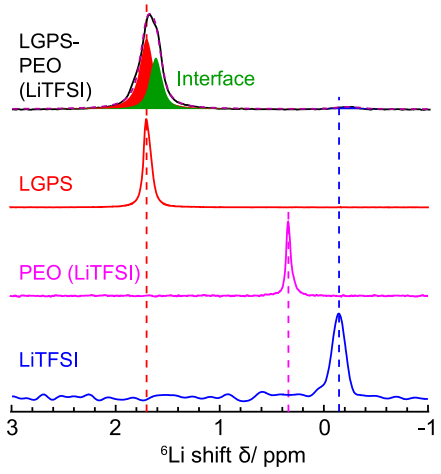

Figure 2. ^{6}Li magic-angle-spinning (MAS) NMR revealing local structural environments in pure LiTFSI salt, LiTFSI in PEO, pure LGPS, and LGPS-PEO (LiTFSI) hybrid films. All the spectra are averaged over 512 scans and a 1.0 Hz Lorentzian line broadening is applied.

DOI: 10.1021/acsaem.8b02008
ACS Appl. Energy Mater. 2019, 2, 1452−1459

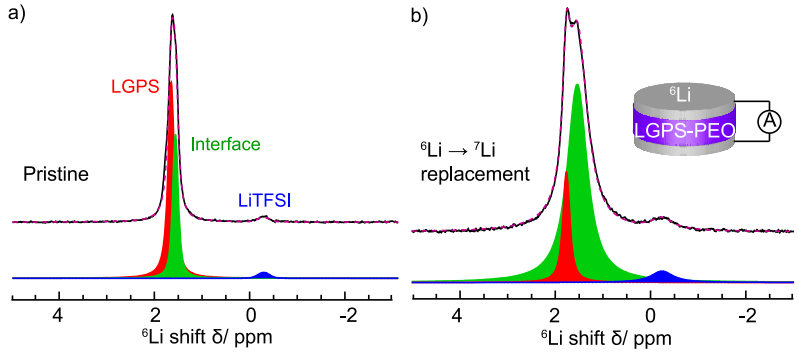

Figure 3. Li-ion transport pathways in LGPS-PEO (LiTFSI) hybrid electrolytes probed with $^{6}Li \rightarrow {}^{7}Li$ tracer-exchange NMR. The participating structural elements in Li-ion transport are revealed by ^{6}Li enrichment after tracer-exchange. ^{6}Li MAS NMR of an LGPS-PEO (LiTFSI) hybrid electrolyte film before (a) and after (b) $^{6}Li \rightarrow {}^{7}Li$ tracer-exchange. The spectral simulations with assignments of the NMR resonances are also shown. A schematic of the symmetric cell used for electrochemically driven tracer-exchange experiments is displayed, which is composed of an LGPS-PEO (LiTFSI) hybrid electrolyte film sandwiched by two pieces of ^{6}Li metal foils.

the LGPS-PEO interfaces. The ^{6}Li resonance from LGPS in pristine LGPS-PEO (LiTFSI) remains at 1.70 ppm and sees significant broadening. A new component appears at 1.60 ppm, as a right shoulder to the 1.70-ppm LGPS resonance. The similar chemical shift of the new resonance to that of Li in LGPS, but larger line width, suggests that this 1.60-ppm component comes from LGPS at the interface with PEO. To confirm the identity of this 1.60-ppm broad resonance, the relative distance of this 1.60-ppm resonance to PEO is determined with $^{1}H-{}^{6}Li$ cross-polarization (CP) experiments, in which the polarization is transferred from ^{1}H in PEO to ^{6}Li in various structural environments, and the transfer efficiency is strongly distance dependent. The $^{1}H-{}^{6}Li$ CP NMR results as a function of cross-polarization contact time are shown in Figure S2. The LiTFSI resonance at −0.16 ppm is observed in the $^{6}Li\{^{1}H\}$ CP spectra as expected due to the close distance of LiTFSI with PEO. In addition, a weak and broad signal from 1.60 ppm is also seen, but the 1.70-ppm resonance from bulk LGPS is not observed, which suggests that this 1.60-ppm resonance is from Li relatively closer to PEO compared with bulk LGPS. This confirms that the broad 1.60-ppm resonance is from LGPS at interfaces with PEO. Quantitative spectral analysis (Figure 3a and Table 1) reveals that Li from bulk LGPS, at LGPS-PEO interfaces, and in LiTFSI account for 60.9%, 36.7%, and 2.4%, respectively, in the 70 wt % LGPS-PEO (LiTFSI) hybrid with the ratio of EO/Li (from LiTFSI) = 9:1.

Table 1. Quantification Results[a] of ^{6}Li Enrichment in the LGPS-PEO (LiTFSI) Film before and after Tracer-Exchange, Based on ^{6}Li NMR in Figure 3

	bulk LGPS	LGPS at interfaces	LiTFSI	total
Pristine	60.9	36.7	2.4	100
After $^{6}Li \rightarrow {}^{7}Li$ tracer-exchange	21.4	112.5	7.2	141
^{6}Li enhancement	−39.5	75.7	4.8	41

[a]In percent (%).

To investigate the roles that each component of LGPS-PEO (LiTFSI) plays in Li-ion transport, tracer-exchange Li NMR is employed, which combines $^{6}Li \rightarrow {}^{7}Li$ isotope exchange with high-resolution ^{6}Li NMR to determine Li-ion transport pathways in complex materials (Figure 3). $^{6}Li \rightarrow {}^{7}Li$ isotope exchange is driven by a biased electric potential applied upon on a symmetric cell made of ^{6}Li/LGPS-PEO (LiTFSI)/^{6}Li (Figure 3b). ^{7}Li is naturally abundant, accounting for 92.4%, while ^{6}Li is only 7.6%. Under the biased electric potential, ^{6}Li ions from the ^{6}Li-enriched metal electrodes are driven to pass through the hybrid electrolyte, partially replacing ^{7}Li or occupying empty/interstitial sites on their paths. In other words, the structural components that participate in Li-ion transport will be ^{6}Li-enriched after the tracer-exchange process. Thus, Li-ion transport pathways encoded with specific chemical information can be determined by comparing ^{6}Li-enrichment of different structural sites before and after tracer-exchange. Figure 3 exhibits the ^{6}Li NMR spectra together with spectral simulation of LGPS-PEO (LiTFSI) before and after $^{6}Li \rightarrow {}^{7}Li$ tracer-exchange. An increase in the relative ^{6}Li amount of the interfacial Li and LiTFSI components is observed in conjunction with the decrease seen in the bulk LGPS. The quantitative ^{6}Li enhancement levels are evaluated by calculating the changes of ^{6}Li amount in each structural component before and after tracer-exchange (Figure 3), and the results are listed in Table 1. The total amount of ^{6}Li in LGPS-PEO (LiTFSI) is increased by a factor of 1.41 after tracer-exchange. ^{6}Li amount both at LGPS-PEO interfaces and in LiTFSI is increased by nearly 3-fold, suggesting that Li-ion transport takes place mainly at the interfaces. LiTFSI of a small amount also contributes to ion conduction. A decrease of ^{6}Li amount is seen in bulk LGPS, which is likely due to the further disintegration of the bulk structure during electrochemical cycling. This is supported by the broadening of the ^{7}Li NMR resonance from LGPS after electrochemical cycling (Figure S3).

As Li ions at LGPS-PEO interfaces play the major role in ion conduction within the LGPS-PEO (LiTFSI) hybrids suggested by the tracer-exchange NMR results, the impact of LGPS and LiTFSI content on Li at interfaces in the hybrids is investigated. LGPS-PEO (LiTFSI) hybrids with 50, 70, and 90 wt % LGPS and the same EO/Li (from LiTFSI) = 9:1 are prepared. The volume percentage (vol %) of each component in these hybrid electrolytes is listed in Table S2, using the densities of LGPS (2.00 g cm^{-3}), PEO (1.21 g cm^{-3}), and LiTFSI (1.33 g cm^{-3}).[17] High-resolution ^{6}Li NMR is performed on these hybrid samples in order to quantify the Li content at interfaces. As shown in Figure 4, a very limited amount of Li at interfaces is observed for 50 and 90 wt %

DOI: 10.1021/acsaem.8b02008
ACS Appl. Energy Mater. 2019, 2, 1452−1459

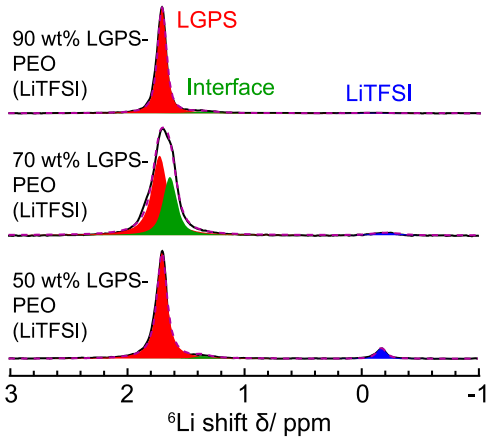

Figure 4. Impact of LGPS fraction in the hybrid electrolytes on Li at PEO-LGPS interfaces revealed by ^{6}Li NMR. From top to bottom, the MAS ^{6}Li NMR of 90, 70, and 50 wt % LGPS-PEO (LiTFSI) with the same mole ratio of EO/Li, i.e., 9:1.

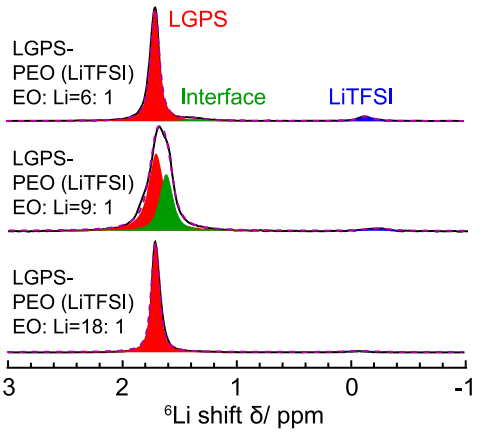

Figure 5. Impact of LiTFSI salt content in the hybrid electrolytes on Li at PEO-LGPS interfaces revealed by ^{6}Li NMR. From top to bottom, the ^{6}Li MAS NMR of 70 wt % LGPS-PEO (LiTFSI) with the mole ratio of EO/Li to be 6:1, 9:1, and 18:1.

LGPS-PEO (LiTFSI) hybrids, despite the non-negligible volume fractions of LGPS (Table S2). In addition to volume fraction, effective mixing of LGPS and PEO (LiTFSI) is also crucial for creating interfaces.[18] It turns out that for the 50 and 90 wt % cases, the mixing of LGPS with PEO is not as good as the 70 wt % sample. To confirm the reproducibility of the composite electrolyte fabrication, the 50 wt % LGPS-PEO (LiTFSI) (9:1) is remade; the result in Figure S4 shows again limited formation of interface, consistent with our prior results. Therefore, the evaluation of the formation of interface simply based on the volume fraction of LGPS is insufficient, and detailed NMR characterizations of interface become necessary. It is worth noting that the LiTFSI amount observed in ^{6}Li NMR (Figure 4) increases with the PEO fractions in the hybrids as expected with fixed EO/Li (from LiTFSI) = 9:1. Furthermore, LiTFSI resonance from 50 wt % LGPS-PEO (LiTFSI) is much sharper compared with that of 70 wt % LGPS-PEO (LiTFSI). LiTFSI in 50 wt % LGPS-PEO (LiTFSI) is expected to distribute in the PEO phase only due to the lack of interfaces between PEO and LGPS; therefore, the local structural environment for LiTFSI is relatively uniform. For LiTFSI in 70 wt % LGPS-PEO (LiTFSI), LiTFSI can possibly locate at LGPS-PEO interfaces. This brings about the following investigation on the impact of LiTFSI content on LGPS-PEO interface formation, where 70 wt % LGPS-PEO (LiTFSI) hybrids with EO/Li (from LiTFSI) = 18:1, 9:1, and 6:1 are fabricated, and the corresponding ^{6}Li NMR spectra are shown in Figure 5. In the hybrids with EO/Li (from LiTFSI) = 18:1 and 6:1, only a very small amount of Li at LGPS-PEO interfaces is observed, compared with hybrids containing EO/Li (from LiTFSI) = 9:1. It suggests that LiTFSI content also has significant effects on LGPS-PEO interfaces. With low LiTFSI content, such as EO/Li (from LiTFSI) = 18:1, the effect on interface formation is small. At high LiTFSI content, such as EO/Li (from LiTFSI) = 6:1, the LiTFSI partially aggregates, suggested by the sharp ^{6}Li resonance in Figure 5.[19,20] Another reason for the observed limited LGPS-PEO interface formation at high LiTFSI content is that interactions between LiTFSI and PEO alter the mechanical properties of PEO matrix, making it more rigid and less "cementing" when mixed with LGPS, as evidenced by the reduced flexibility of 70 wt % LGPS-PEO (LiTFSI) (6:1) hybrid film. In summary, both the composition and LiTFSI salt content in the LGPS-PEO (LiTFSI) impact the LGPS-PEO interface formation. In addition, the fabrication process is also expected to affect the interface chemistry. For instance, different mixing methods result in varied outcomes; a 70 wt % LGPS-PEO (LiTFSI) (9:1) hybrid film is prepared through stirring the mixture of LGPS and PEO (LiTFSI) for 2 h instead of ball-milling. The ^{6}Li MAS NMR comparison of 70 wt % LGPS-PEO (LiTFSI) (9:1) hybrid films prepared through ball-milling and stirring are shown in Figure S5. The film prepared through stirring has a very small amount of interface, and the ionic conductivity is 0.078 mS cm^{-1}, which is lower than that of the film prepared through ball-milling, which is 0.22 mS cm^{-1}. Fabrication methods such as ball-milling to facilitate effective mixing are helpful to create synergistic interface for ion conduction.[21−23]

The conductivity of LGPS-PEO (LiTFSI) hybrid films is measured with EIS. As the potential residual solvent in the electrolytes may affect their conductivity, and to determine the amount of possible residual solvent in the samples after drying, TGA experiments were performed. The boiling temperature of the solvent, anhydrous acetonitrile, was 82 °C. Based on the TGA results (Figure S6), the weight loss below 100 °C of PEO, PEO (LiTFSI), and LGPS-PEO (LiTFSI) films is around 1.0%. Therefore, the solvent contribution to the final conductivity is estimated to be small.

The conductivity results of the hybrid films are shown in Figures 6 and S7.With increasing LGPS content in the hybrid electrolytes, the overall conductivity increases and reaches a maximum at 70 wt % of LGPS with a conductivity of 0.22 mS cm^{-1}. When the amount of LGPS is further increased to 90 wt %, the conductivity decreases to 0.074 mS cm^{-1}. The trend of conductivity correlates with the amount of LGPS-PEO interfaces (Figure 6a). A similar pattern is observed for conductivity with increasing the LiTFSI salt content in the hybrids while maintaining the same composition of 70 wt % LGPS-PEO (Figure 6b). The conductivity increases with LiTFSI content and reaches the maximum of 0.22 mS cm^{-1} when EO/Li (from LiTFSI) = 9:1. Further increase in LiTFSI content to EO/Li (from LiTFSI) = 6:1 results in more than 10-fold decrease in conductivity (Figure 6b). The trend in conductivity variation echoes with that for interface changes with LGPS and LiTFSI content in the hybrids. It is consistent with the tracer-exchange Li NMR results, revealing that Li-ion

DOI: 10.1021/acsaem.8b02008
ACS Appl. Energy Mater. 2019, 2, 1452−1459

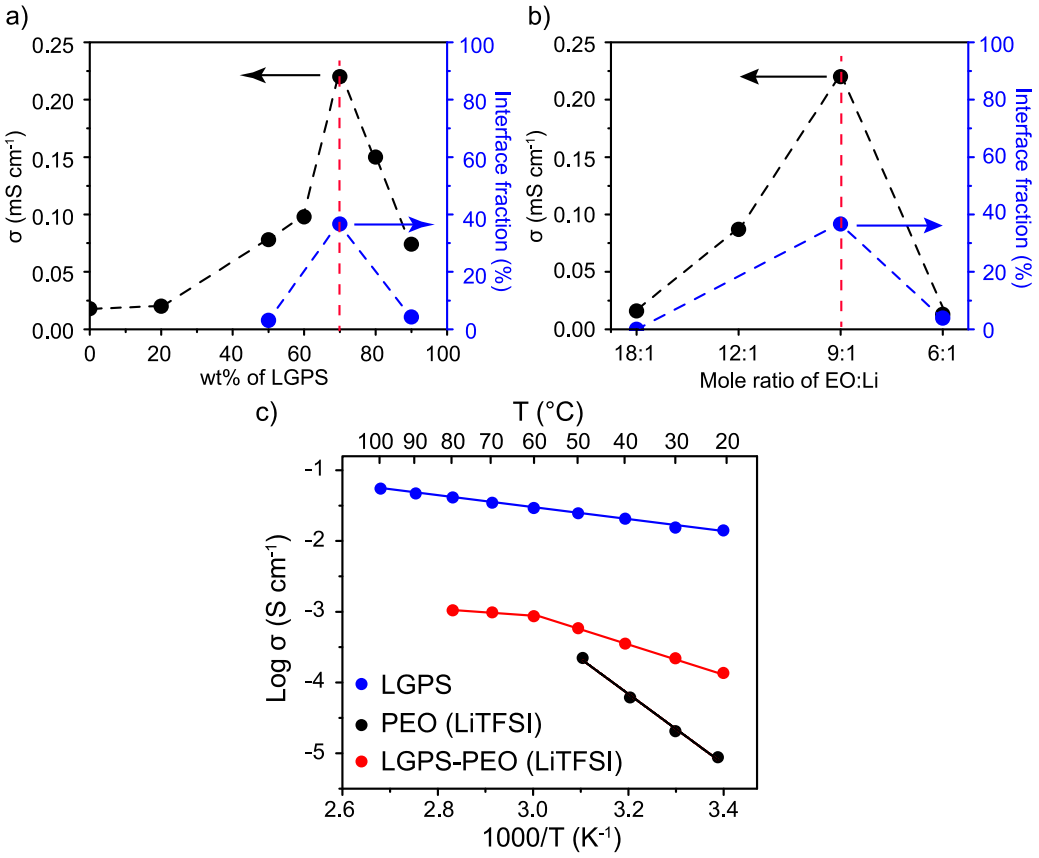

Figure 6. (a) The conductivity and interface fraction of LGPS-PEO (LiTFSI) (9:1) as a function of the weight percent of LGPS, i.e., 20, 50, 60, 70, 80, and 90 wt %. (b) The conductivity and interface fraction of 70 wt % LGPS-PEO (LiTFSI) as a function of the mole ratio of EO to Li, i.e., 18:1, 12:1, 9:1, and 6:1. The conductivity in (a) and (b) was measured at 22 °C. (c) The Arrhenius plots of LGPS, PEO (LiTFSI) (9:1), and 70 wt % LGPS-PEO (LiTFSI) (9:1) electrolytes.

transport within the LGPS-PEO (LiTFSI) hybrid films mainly occurs at LGPS-PEO interfaces.

The 70 wt % LGPS-PEO (LiTFSI) hybrid shows distinct advantages over PEO (LiTFSI) in ion conduction. The Arrhenius plots of conductivity as a function of temperature for LGPS, PEO (LiTFSI) (9:1), and 70 wt % LGPS-PEO (LiTFSI) (9:1) electrolytes are displayed in Figure 6c. The ionic conductivity of 70 wt % LGPS-PEO (LiTFSI) (9:1) is 0.22 mS cm^{-1}, which is 25 times higher than that of PEO (LiTFSI) (8.75×10^{-3} mS cm^{-1}) and lower than that of LGPS (14 mS cm^{-1}). The contribution of LGPS in the LGPS-PEO (LiTFSI) hybrids is manifested in the formation of ion-conducting LGPS-PEO interfaces and provision of active Li^+ at the interfaces. The activation energies (E_a) for Li-ion transport in LGPS and PEO (LiTFSI) (9:1) are 0.17 and 0.99 eV, respectively.[24,25] The E_a of 70 wt % LGPS-PEO (LiTFSI) (9:1) is 0.40 eV in the temperature range of 20−50 °C and 0.10 eV between 60 and 80 °C. To understand the change of E_a in the 70 wt % LGPS-PEO (LiTFSI) (9:1), differential scanning calorimetry (DSC) measurements of pure PEO, PEO (LiTFSI) (9:1), and 70 wt % LGPS-PEO (LiTFSI) (9:1) were performed (Figure S6). The melting temperature (T_m) of pure PEO is 72 °C. The addition of LiTFSI in PEO (LiTFSI) (9:1) decreases the T_m of to 52 °C.[26,27] The E_a change of 70 wt % LGPS-PEO (9:1) is due to the melting of the PEO phase. It is worth noting that unlike polymer electrolytes, the thermal history of the composite electrolytes does not significantly affect their conductivity. The comparison of the conductivity measurements performed during heating and cooling processes of 70 wt % LGPS-PEO (LiTFSI) (9:1) is shown in Figure S8. These two sets of data resemble each other within error margins.

The advantages of the composites electrolytes also manifest in the enhanced transference number (T_{Li+}). As shown in Figure S9 and Table S3. The T_{Li+} values of PEO (LiTFSI) (9:1) and LGPS are 0.09 and 0.99, respectively.[28−30] In LGPS-PEO (LiTFSI) hybrid electrolytes, T_{Li+} values are higher with more LGPS,[31,32] and a T_{Li+} value of 0.91 can be achieved for 90 wt % LGPS-PEO (LiTFSI) (9:1).

It is worth noting that the results obtained for LGPS-PEO (LiTFSI) are different from those for $Li_7La_3Zr_2O_{12}$ (LLZO)-PEO (LiTFSI) hybrid electrolytes. In LLZO-PEO (LiTFSI) hybrid electrolytes, no ion-conducting interfaces are formed; therefore, Li-ion transport takes place either in the modified PEO phase or through the percolated network of LLZO particles.[7,13,33] The difference between LGPS-PEO (LiTFSI) and LLZO-PEO (LiTFSI) hybrids is likely originated from the difference in mechanical properties of LGPS and LLZO. For oxide conductors such as LLZO, they are rigid and difficult to closely integrate with PEO, and therefore, the formation of interfaces is limited. This is evidenced from our prior NMR studies of LLZO-PEO (LiTFSI) for Li-ion conduction. LGPS is soft and cementing, and thus the formation of ion-conducting interfaces with PEO is less challenging. An important question regarding what characteristics of inorganic−organic interfaces, including the distance and inter-

DOI: 10.1021/acsaem.8b02008
ACS Appl. Energy Mater. 2019, 2, 1452−1459

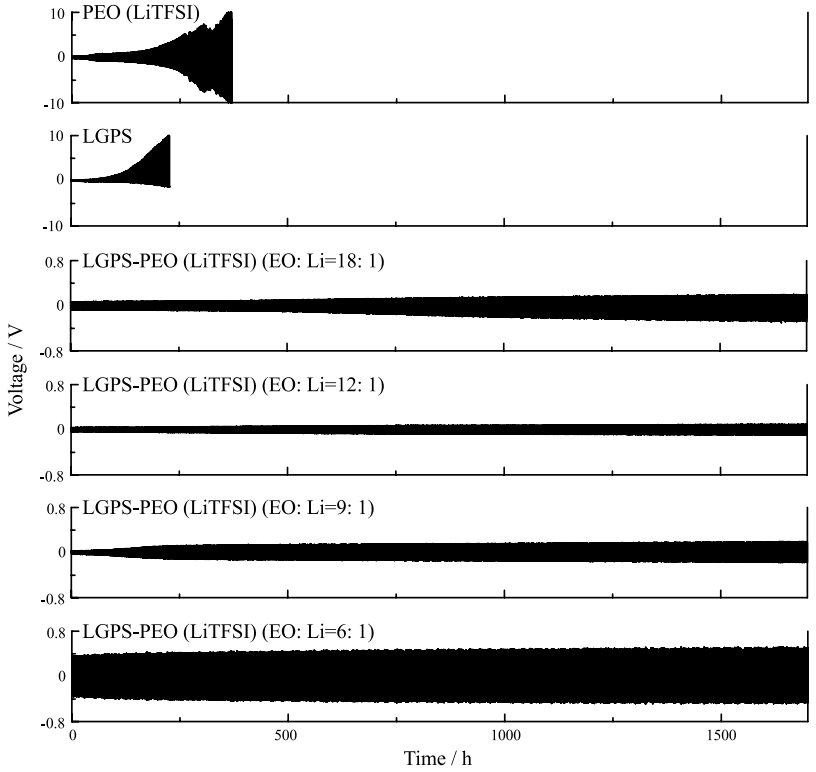

Figure 7. Electrochemical cycling stability against Li of PEO (LiTFSI), LGPS, and 70 wt % LGPS-PEO (LiTFSI) hybrid electrolyte with mole ratios of EO/Li to be 18:1, 12:1, 9:1, and 6:1.

actions between the two comprising moieties, will result in fast ion conduction requires systematic studies in the near future.

Li metal is considered the ultimate anode for Li-ion batteries due to its high theoretical specific capacity (3860 mA h g^{-1}), low negative electrochemical potential (−3.04 V vs the standard hydrogen electrode), and lightweight properties (0.59 g cm^{-3}).[34] To test the long-term electrochemical stability of LGPS-PEO (LiTFSI) hybrid electrolytes against Li metal and compare it with that of pure PEO (LiTFSI) and LGPS, symmetric battery cells are made of PEO (LiTFSI), LGPS, and LGPS-PEO (LiTFSI) as electrolytes and Li metal as electrodes, and the symmetric cells are cycled with a constant current density of 10 μA cm^{-2} (Figure 7). The voltage of the Li/PEO (LiTFSI)/Li cell increases steeply to 10 V after cycling for 370 h, and the voltage of the Li/LGPS/Li cell reaches 10 V after 224 h. LGPS is chemically and electrochemically unstable against Li metal. A recent 3D ^{7}Li magnetic resonance imaging (MRI) study on Li/LGPS/Li symmetric cell has revealed significant Li loss at the LGPS/Li interface and heterogeneous distribution of Li in the bulk LGPS during electrochemical cycling, which results in large interfacial and bulk resistance.[12] LGPS-PEO (LiTFSI) hybrid electrolytes exhibit improved cycling performance against Li metal, compared with PEO and LGPS. The best performance is found for the composition of 70 wt % LGPS-PEO (LiTFSI) (EO/Li = 12:1). The initial voltage of the Li|LGPS-PEO (EO/Li = 12:1)|Li cell is 0.03 V and slightly increases to 0.083 V after 1700 h. The integration of LGPS and PEO in the hybrid electrolytes allows ion transport through LGPS-PEO interfaces, which largely limits direct contact between Li metal and unstable LGPS and thus enhances the stability. In addition, interfacial LGPS as the ion transport media is a single-ion conductor and does not contain free anions; this is beneficial to achieving large transference number, high conductivity, and homogeneous distribution of Li ions. These factors also help enhance the long-term cycling stability of hybrid electrolytes.[6]

The concentration of LiTFSI salts has effects on the electrochemical stability of LGPS-PEO (LiTFSI) against Li metal. As mentioned above, 70 wt % LGPS-PEO (LiTFSI) (EO/Li = 12:1) delivers the best long-term performance in this study. At low or high Li salts contents, for instance, LGPS-PEO (LiTFSI) (EO/Li = 18:1) and LGPS-PEO (LiTFSI) (EO/Li = 6:1), the cell resistance is large due to low ionic conductivity of LGPS-PEO (LiTFSI) (EO/Li = 18:1) and LGPS-PEO (LiTFSI) (EO/Li = 6:1). The ionic conductivity of LGPS-PEO (LiTFSI) (EO/Li = 9:1) is high (0.22 mS cm^{-1}); therefore, the initial voltage of Li|LGPS-PEO (LiTFSI) (EO/Li = 9:1)|Li is low, at 0.02 V, but the voltage increases fairly rapidly to 0.20 V after 1700 h of electrochemical cycling. The determination of optimal Li salt content in hybrid electrolytes may need to strike a balance between achieving the highest conductivity and the long-term cycling stability.

■ CONCLUSIONS

LGPS-PEO (LiTFSI) hybrid electrolytes have been prepared. The local structural environments of Li ions within the hybrids are identified with high-resolution solid-state ^{6}Li NMR. Li ions transport via LGPS-PEO interfaces in the hybrids, determined with tracer-exchange Li NMR. The effects of composition, LiTFSI salt content, and the fabrication process of LGPS-PEO (LiTFSI) hybrid electrolytes on the LGPS-PEO interface formation are examined, which reveals that 70 wt % LGPS-PEO (LiTFSI) (EO/ Li = 9:1) prepared with ball-milling results in the maximum interface amount. The measured ionic conductivities of LGPS-PEO (LiTFSI) hybrid electrolytes positively correlate with the amount of LGPS-PEO interface

DOI: 10.1021/acsaem.8b02008
ACS Appl. Energy Mater. 2019, 2, 1452−1459

quantified by ^{6}Li NMR. The highest ionic conductivity of 0.22 mS cm^{-1} is achieved in 70 wt % LGPS-PEO (LiTFSI) (EO/Li = 9:1). LGPS-PEO (LiTFSI) also shows an enhanced Li^+ transference number and long-term cycling stability against Li metal compared with pure LGPS and PEO (LiTFSI). The impact of LiTFSI content in the hybrid on cycling stability is also examined with the highest stability found with 70 wt % LGPS-PEO (LiTFSI) (EO/Li = 12:1). This study demonstrates the important roles that interfaces play in regulating ion conductions in hybrid solid electrolytes. Highly conductive and stable solid electrolytes are key to safe energy storage technologies of high energy and power densities.

■ ASSOCIATED CONTENT

Supporting Information

The Supporting Information is available free of charge on the ACS Publications website at DOI: 10.1021/acsaem.8b02008.

SEM, ^{1}H−^{6}Li cross-polarization NMR, parameters for ^{6}Li NMR fitting, ^{6}Li NMR, ^{7}Li NMR, TGA, DSC, and EIS analyses (PDF)

■ AUTHOR INFORMATION

Corresponding Author

*E-mail: hu@chem.fsu.edu.

ORCID

Jin Zheng: 0000-0003-1114-1135

Yan-Yan Hu: 0000-0003-0677-5897

Notes

The authors declare no competing financial interest.

■ ACKNOWLEDGMENTS

This study was sponsored by the National Science Foundation (DMR-1808517) and the Marion Milligan Mason Award, AAAS. All of the solid-state NMR experiments were carried out at the NHMFL, which is supported by the National Science Foundation Cooperative Agreement (DMR-1644779) and the State of Florida. We appreciate Dr. Shou-Hang Bo and Yifan Wu from Shanghai Jiao Tong University for help in collecting the SEM image.

■ REFERENCES

(1) Tarascon, J.-M.; Armand, M. Issues and Challenges Facing Rechargeable Lithium Batteries. *Nature* **2001**, *414*, 359−367.

(2) Gao, Z.; Sun, H.; Fu, L.; Ye, F.; Zhang, Y.; Luo, W.; Huang, Y. Promises, Challenges, and Recent Progress of Inorganic Solid-State Electrolytes for All-Solid-State Lithium Batteries. *Adv. Mater.* **2018**, *30*, 1705702.

(3) Fan, L.; Wei, S.; Li, S.; Li, Q.; Lu, Y. Recent Progress of the Solid-State Electrolytes for High-Energy Metal-Based Batteries. *Adv. Energy Mater.* **2018**, *8*, 1702657.

(4) Xue, Z.; He, D.; Xie, X. Poly(Ethylene Oxide)-Based Electrolytes for Lithium-Ion Batteries. *J. Mater. Chem. A* **2015**, *3*, 19218−19253.

(5) Keller, M.; Varzi, A.; Passerini, S. Hybrid Electrolytes for Lithium Metal Batteries. *J. Power Sources* **2018**, *392*, 206−225.

(6) Zhao, C.-Z.; Zhang, X.-Q.; Cheng, X.-B.; Zhang, R.; Xu, R.; Chen, P.-Y.; Peng, H.-J.; Huang, J.-Q.; Zhang, Q. An Anion-Immobilized Composite Electrolyte for Dendrite-Free Lithium Metal Anodes. *Proc. Natl. Acad. Sci. U. S. A.* **2017**, *114*, 11069−11074.

(7) Zhang, X.; Liu, T.; Zhang, S.; Huang, X.; Xu, B.; Lin, Y.; Xu, B.; Li, L.; Nan, C.-W.; Shen, Y. Synergistic Coupling between $Li_{6.75}La_3Zr_{1.75}Ta_{0.25}O_{12}$ and Poly(Vinylidene Fluoride) Induces High Ionic Conductivity, Mechanical Strength, and Thermal Stability of Solid Composite Electrolytes. *J. Am. Chem. Soc.* **2017**, *139*, 13779−13785.

(8) Li, Y.; Xu, B.; Xu, H.; Duan, H.; Lü, X.; Xin, S.; Zhou, W.; Xue, L.; Fu, G.; Manthiram, A.; Goodenough, J. B. Hybrid Polymer/Garnet Electrolyte with a Small Interfacial Resistance for Lithium-Ion Batteries. *Angew. Chem., Int. Ed.* **2017**, *56*, 753−756.

(9) Kato, Y.; Hori, S.; Saito, T.; Suzuki, K.; Hirayama, M.; Mitsui, A.; Yonemura, M.; Iba, H.; Kanno, R. High-Power All-Solid-State Batteries Using Sulfide Superionic Conductors. *Nat. Energy* **2016**, *1*, 16030.

(10) Kamaya, N.; Homma, K.; Yamakawa, Y.; Hirayama, M.; Kanno, R.; Yonemura, M.; Kamiyama, T.; Kato, Y.; Hama, S.; Kawamoto, K.; Mitsui, A. A Lithium Superionic Conductor. *Nat. Mater.* **2011**, *10*, 682−686.

(11) Mo, Y.; Ong, S. P.; Ceder, G. First Principles Study of the $Li_{10}GeP_2S_{12}$ Lithium Super Ionic Conductor Material. *Chem. Mater.* **2012**, *24*, 15−17.

(12) Chien, P.-H.; Feng, X.; Tang, M.; Rosenberg, J. T.; O'Neill, S.; Zheng, J.; Grant, S. C.; Hu, Y.-Y. Li Distribution Heterogeneity in Solid Electrolyte $Li_{10}GeP_2S_{12}$ upon Electrochemical Cycling Probed by ^{7}Li MRI. *J. Phys. Chem. Lett.* **2018**, *9*, 1990−1998.

(13) Yang, T.; Zheng, J.; Cheng, Q.; Hu, Y.-Y.; Chan, C. K. Composite Polymer Electrolytes with $Li_7La_3Zr_2O_{12}$ Garnet-Type Nanowires as Ceramic Fillers: Mechanism of Conductivity Enhancement and Role of Doping and Morphology. *ACS Appl. Mater. Interfaces* **2017**, *9*, 21773−21780.

(14) Zheng, J.; Dang, H.; Feng, X.; Chien, P.-H.; Hu, Y.-Y. Li-Ion Transport in a Representative Ceramic−Polymer−Plasticizer Composite Electrolyte: $Li_7La_3Zr_2O_{12}$−Polyethylene Oxide−Tetraethylene Glycol Dimethyl Ether. *J. Mater. Chem. A* **2017**, *5*, 18457−18463.

(15) Zheng, J.; Tang, M.; Hu, Y.-Y. Lithium Ion Pathway within $Li_7La_3Zr_2O_{12}$-Polyethylene Oxide Composite Electrolytes. *Angew. Chem.* **2016**, *128*, 12726−12730.

(16) Zheng, J.; Hu, Y.-Y. New Insights into the Compositional Dependence of Li-Ion Transport in Polymer−Ceramic Composite Electrolytes. *ACS Appl. Mater. Interfaces* **2018**, *10*, 4113−4120.

(17) Wu, B.; Wang, S.; Evans, W. J., IV; Deng, D. Z.; Yang, J.; Xiao, J. Interfacial Behaviours between Lithium Ion Conductors and Electrode Materials in Various Battery Systems. *J. Mater. Chem. A* **2016**, *4*, 15266−15280.

(18) Makokha, A. B.; Moys, M. H.; Muumbo, A. M.; Kiprono, R. J. Optimization of In-Mill Ball Loading and Slurry Solids Concentration in Grinding of UG-2 Ores: A Statistical Experimental Design Approach. *Miner. Eng.* **2012**, *39*, 149−155.

(19) Rey, I.; Lassègues, J. C.; Grondin, J.; Servant, L. Infrared and Raman Study of the PEO-LiTFSI Polymer Electrolyte. *Electrochim. Acta* **1998**, *43*, 1505−1510.

(20) Bakker, A.; Lindgren, J.; Hermansson, K. Polymer Electrolytes Based on Triblock-Copoly(Oxyethylene/Oxypropylene/Oxyethylene) Systems. *Polymer* **1996**, *37*, 1871−1878.

(21) Zheng, J.; Peng, J.; Zheng, Z.; Zhou, M.; Thompson, E.; Yang, J.; Xiao, W. Synthesis and High Temperature Thermoelectric Properties of $Yb_{0.25}Co_4Sb_{12}$-$(Ag_2Te)x(Sb_2Te_3)_{1-x}$ Nanocomposites. *Front. Chem.* **2015**, *3*, 1.

(22) Dudina, D. V.; Lomovsky, O. I.; Valeev, K. R.; Tikhov, S. F.; Boldyreva, N. N.; Salanov, A. N.; Cherepanova, S. V.; Zaikovskii, V. I.; Andreev, A. S.; Lapina, O. B.; Sadykov, V. A. Phase Evolution during Early Stages of Mechanical Alloying of Cu−13wt.% Al Powder Mixtures in a High-Energy Ball Mill. *J. Alloys Compd.* **2015**, *629*, 343−350.

(23) Li, Z. P.; Morigazaki, N.; Liu, B. H.; Suda, S. Preparation of Sodium Borohydride by the Reaction of MgH_2 with Dehydrated Borax through Ball Milling at Room Temperature. *J. Alloys Compd.* **2003**, *349*, 232−236.

(24) Hassoun, J.; Verrelli, R.; Reale, P.; Panero, S.; Mariotto, G.; Greenbaum, S.; Scrosati, B. A Structural, Spectroscopic and Electrochemical Study of a Lithium Ion Conducting $Li_{10}GeP_2S_{12}$ Solid Electrolyte. *J. Power Sources* **2013**, *229*, 117−122.

(25) Tu, Z.; Choudhury, S.; Zachman, M. J.; Wei, S.; Zhang, K.; Kourkoutis, L. F.; Archer, L. A. Designing Artificial Solid-Electrolyte Interphases for Single-Ion and High-Efficiency Transport in Batteries. *Joule* **2017**, *1*, 394−406.
(26) Zheng, Q.; Pesko, D. M.; Savoie, B. M.; Timachova, K.; Hasan, A. L.; Smith, M. C.; Miller, T. F.; Coates, G. W.; Balsara, N. P. Optimizing Ion Transport in Polyether-Based Electrolytes for Lithium Batteries. *Macromolecules* **2018**, *51*, 2847−2858.
(27) Marzantowicz, M.; Dygas, J. R.; Krok, F.; Łasińska, A.; Florjańczyk, Z.; Zygadło-Monikowska, E.; Affek, A. Crystallization and Melting of PEO:LiTFSI Polymer Electrolytes Investigated Simultaneously by Impedance Spectroscopy and Polarizing Microscopy. *Electrochim. Acta* **2005**, *50*, 3969−3977.
(28) Pesko, D. M.; Timachova, K.; Bhattacharya, R.; Smith, M. C.; Villaluenga, I.; Newman, J.; Balsara, N. P. Negative Transference Numbers in Poly(Ethylene Oxide)-Based Electrolytes. *J. Electrochem. Soc.* **2017**, *164*, E3569−E3575.
(29) Pozyczka, K.; Marzantowicz, M.; Dygas, J. R.; Krok, F. Ionic Conductivity And Lithium Transference Number of Poly(ethylene oxide):LiTFSI System. *Electrochim. Acta* **2017**, *227*, 127−135.
(30) Zhao, Y.; Wu, C.; Peng, G.; Chen, X.; Yao, X.; Bai, Y.; Wu, F.; Chen, S.; Xu, X. A New Solid Polymer Electrolyte Incorporating $Li_{10}GeP_2S_{12}$ into a Polyethylene Oxide Matrix for All-Solid-State Lithium Batteries. *J. Power Sources* **2016**, *301*, 47−53.
(31) Yang, L.; Wang, Z.; Feng, Y.; Tan, R.; Zuo, Y.; Gao, R.; Zhao, Y.; Han, L.; Wang, Z.; Pan, F. Flexible Composite Solid Electrolyte Facilitating Highly Stable "Soft Contacting" Li-Electrolyte Interface for Solid State Lithium-Ion Batteries. *Adv. Energy Mater.* **2017**, *7*, 1701437.
(32) Diederichsen, K. M.; McShane, E. J.; McCloskey, B. D. Promising Routes to a High Li^+ Transference Number Electrolyte for Lithium Ion Batteries. *ACS Energy Lett.* **2017**, *2*, 2563−2575.
(33) Zhang, J.; Zang, X.; Wen, H.; Dong, T.; Chai, J.; Li, Y.; Chen, B.; Zhao, J.; Dong, S.; Ma, J.; Yue, L.; Liu, Z.; Guo, X.; Cui, G.; Chen, L. High-Voltage and Free-Standing Poly(Propylene Carbonate)/$Li_{6.75}La_3Zr_{1.75}Ta_{0.25}O_{12}$ Composite Solid Electrolyte for Wide Temperature Range and Flexible Solid Lithium Ion Battery. *J. Mater. Chem. A* **2017**, *5*, 4940−4948.
(34) Lin, D.; Liu, Y.; Cui, Y. Reviving the Lithium Metal Anode for High-Energy Batteries. *Nat. Nanotechnol.* **2017**, *12*, 194−206.

DOI: 10.1021/acsaem.8b02008
ACS Appl. Energy Mater. 2019, 2, 1452−1459